

# Accurate Baryon Acoustic Oscillations reconstruction via semi-discrete optimal transport

Sebastian von Hausegger<sup>1,2,3,\*</sup>, Bruno Levy<sup>2</sup>, and Roya Mohayaee<sup>1,3</sup>

<sup>1</sup>*Rudolf Peierls Centre for Theoretical Physics, University of Oxford,  
Parks Road, Oxford OX1 3PU, United Kingdom*

<sup>2</sup>*Université de Lorraine, CNRS, Inria, LORIA, F-54000 Nancy, France and*

<sup>3</sup>*Institut d'Astrophysique de Paris, CNRS, Sorbonne Université, 98bis Bld Arago, 75014 Paris, France*

(Dated: November 10, 2021)

Optimal transport theory has recently reemerged as a vastly resourceful field of mathematics with elegant applications across physics and computer science. Harnessing methods from geometry processing, we report on the efficient implementation for a specific problem in cosmology — the reconstruction of the linear density field from low redshifts, in particular the recovery of the Baryonic Acoustic Oscillation (BAO) scale. We demonstrate our algorithm's accuracy by retrieving the BAO scale in noise-less cosmological simulations that are dedicated to cancel cosmic variance; we find uncertainties to be reduced by factor of 4.3 compared with performing no reconstruction, and a factor of 3.1 compared with standard reconstruction.

## I. INTRODUCTION

Linear perturbations in the primordial Universe propagate as sound waves through the photon-baryon plasma until light and matter decouple. In a balance of radiation pressure and gravity, the baryon-to-photon and the matter-to-radiation ratios define a correlation length that is imprinted as a distinct feature onto the density fields, detectable in both the Cosmic Microwave Background (CMB) at early and the Large Scale Structure (LSS) at late times [1–3]. However, non-linear clustering of galaxies at low redshifts distort this imprint and therewith impedes unbiased detection [4], calling for methods to undo these non-linear effects, to ‘reconstruct’ the linear density field, and thereby to enable accurate and precise measurement [5]. This so-called Baryon Acoustic Oscillation (BAO) scale serves as a unique tool to map the expansion history of the Universe, and hence has taken up a central role in cosmological analyses; most notably, its detection [6, 7] has provided constraints on standard quantities such as the Hubble constant and dark energy density [8], with promising capabilities to, with future observations, even constrain more nuanced theories of, e.g., light degrees-of-freedom [9]. Therefore, and especially in light of present and upcoming large galaxy surveys [10], the development of fast, accurate, and scalable reconstruction methods is highly relevant to optimizing the yield of LSS studies. As a prime example of the wide and successful applicability of modern Optimal transport theory, this *Letter* promotes a recent implementation of one such method.

Optimal transport theory describes mappings between probability measures that minimise a total cost function while satisfying a volume conservation constraint [11, 12]. Recent advances in both the mathematical and algorithmic aspects of the theory paved the way for break-

throughs in various fields, such as artificial intelligence, economics, meteorology, biology, and physics — due to the universality of processes minimizing an action. In the context of this work, we exploit natural connections between optimal transport and physics [13, 14]: the to-be-minimised quantity and volume conservation are an action integral and the continuity equation respectively. The Lagrange multiplier associated with the constraint turns out to be the gravitational potential.

Drawing from and building on all these advances, we recently developed a deterministic algorithm [14] that efficiently reconstructs the sought-for linear density field. After having fully characterized its behavior in Ref. [14], we here focus on the accuracy with which it retrieves the BAO scale by applying it to noise-free cosmic variance cancelling cosmological simulations generated with the FastPM [15] algorithm.

This *Letter* recapitulates the mathematical basis of our method, illustrates its particular application to cosmological density field reconstruction, and finally showcases its excellent results in comparison with standard reconstruction by the use of noise-free cosmic variance cancelling cosmological simulations.

## II. MONGE-AMPÈRE-KANTOROVICH RECONSTRUCTION

Monge-Ampère-Kantorovich (MAK) reconstruction uniquely determines the Lagrangian trajectories of a given Eulerian distribution of particle positions by solving an optimal transport (OT) problem [14, 16]. To this effect, consider self-gravitating matter in an Einstein-de Sitter universe, where particle trajectories are the solution to extremizing the action  $I$  subject to the Poisson equation, mass conservation and appropriate boundary conditions,

$$I = \frac{1}{2} \int_{\tau_i}^{\tau_f} \int_V \left( \rho |\mathbf{v}|^2 + \frac{3}{2} |\nabla_x \phi|^2 \right) \tau^{3/2} d^3x d\tau. \quad (1)$$

\* sebastian.vonhausegger@physics.ox.ac.uk

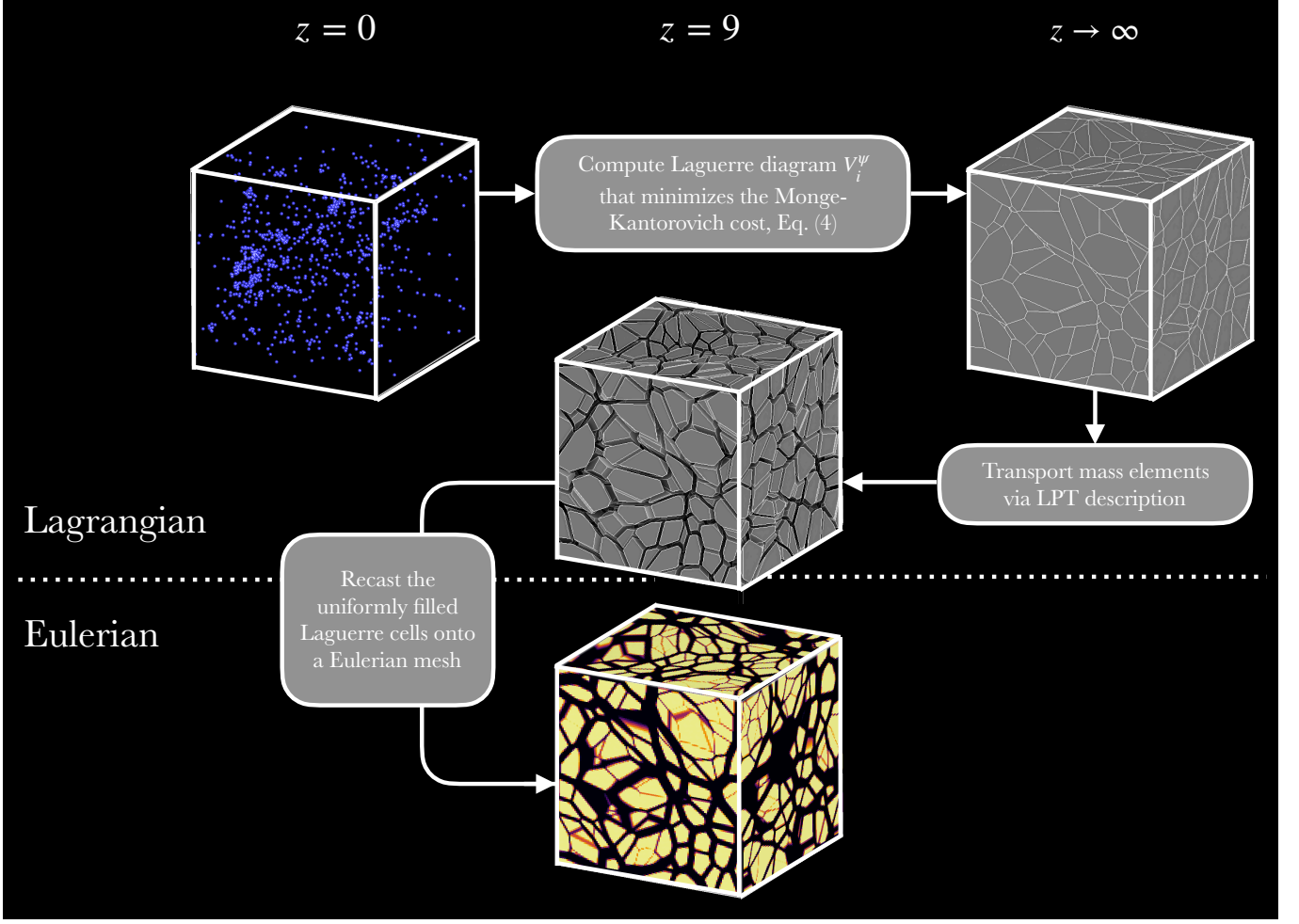


FIG. 1. Semi-discrete Monge-Ampère-Kantorovich Reconstruction. Illustration of the reconstruction’s flow beginning with an input of point masses at  $\tau_F$  (here  $z = 0$ ) that are mapped to their corresponding regions at  $\tau_I$  (here  $z \rightarrow \infty$ ) from where they draw their mass through gravitational collapse. The regions are the polyhedral cells defined by the Laguerre diagram as defined in the main body. In a subsequent step the cells evolve until a time  $\tau_F > \tau > \tau_I$  (here  $z = 9$ ) and according to a LPT description – in the present paper the Zel’dovich approximation. In the final step a mass density is expressed on a Eulerian mesh.

Here,  $\mathbf{x} = \mathbf{x}(\mathbf{q}, \tau)$  are the trajectories in Lagrangian coordinates of particles initially at  $\mathbf{q}$ ,  $\mathbf{v}$  is the Eulerian, co-moving velocity field,  $\rho$  is the Eulerian density field, and  $\phi$  is the gravitational potential. Serving as a time variable,  $\tau$  denotes the amplitude of the growing linear mode, normalized such that initially  $\tau_I = 0$  and finally  $\tau_F = 1$ . Correspondingly, the final density  $\rho(\tau_F)$  is considered to have evolved from an initially uniform state,  $\rho(\tau_I) = 1$ . Ultimately, we aim to recover the (linear) density field at high redshift, or  $\tau = \tau_I + \epsilon$ ,  $\epsilon \ll 1$ , from a low-redshift, or present-time distribution of clustered matter. In practice, this will require finding the optimal map that assigns initial positions  $\mathbf{q}$  to the input particle positions  $\mathbf{x}(\mathbf{q}, \tau_F)$ .

Linearizing around the stationary points of the action, Eq. (1), one finds only the kinetic term to remain, resulting in uniform rectilinear motion [17], exactly as in the Zel’dovich approximation [18]. Interestingly, this case is

proven [19] to be equivalent to the  $L_2$  Monge-Kantorovich optimal transport problem [20],

$$\inf_{\mathbf{x}_F} \int_V \rho(\mathbf{q}) |\mathbf{x}_F(\mathbf{q}) - \mathbf{q}|^2 d^3q, \quad (2)$$

in which the integrated squared distance is minimized, subject to an initially constant density and mass conservation,  $\rho_I(\mathbf{x})/\rho_F(\mathbf{q}) = \det[d^3x/d^3q]$ . The optimal assignment map  $\mathbf{q} \mapsto \mathbf{x}(\mathbf{q})$  turns out to be uniquely determined as the gradient of a convex scalar function, the Kantorovich potential  $\Phi$  [21]. One finds  $\Phi$  by solving the Monge-Ampère equation,

$$\frac{\rho_I(\mathbf{x})}{\rho_F(\mathbf{q})} = \det \left[ \frac{\partial^2 \Phi}{\partial q_i \partial q_j} \right]. \quad (3)$$

The particle trajectories are entirely determined by the initial gravitational potential  $\phi$ , that can be obtained

easily from the Lagrange multiplier of mass conservation, the Kantorovich potential,  $\Phi = 1/2 \mathbf{q}^2 - \phi_I$ . Note that the potential's convexity commands the absence of shell-crossing during structure formation (see [14] for details). In this respect, we also note that the demand for a convex potential allows for more general trajectories than those governed by above Zel'dovich approximation. While numerical methods for approximately solving the Monge-Ampère equation have been devised [22–24], elegant algorithmic developments in computer science allow for efficiently constructing exact solutions.

Previous reconstruction methods that exactly solve the Monge-Ampère equation [13, 16] considered a *discrete* version of the Monge-Kantorovich problem, i.e. to find the permutation  $j(i)$  between a finite set of  $N$  homogeneously distributed particle positions  $(\mathbf{q}_j)_{j=1}^N$  at  $\tau_I$  and their corresponding positions  $(\mathbf{x}_i)_{i=1}^N$  at  $\tau_F$  that minimizes  $\sum_i |\mathbf{x}_{i(j)} - \mathbf{q}_j|^2$  (this minimal distance is called the Wasserstein distance). Efficient combinatorial methods [25] avoid exploring the full set of  $N!$  possible permutations; however, they still scale as  $\sim N^2 \log(N)$ , rendering such algorithms increasingly unfeasible for larger data sets. However, exploiting the variational nature of the Monge-Kantorovich problem, the present *semi-discrete* approach replaces this exhaustive combinatorial search by the optimization of a well-behaved (smooth and concave) objective function, simultaneously making use of the geometric structure of the setting.

Instead of representing the initial condition as a discrete set of points  $(\mathbf{q}_j)_{j=1}^N$ , we consider it as a continuum. This means that instead of a single point  $\mathbf{q}_i$  a region of space is mapped to each  $\mathbf{x}_i$ . As before, the map that assigns these regions to their corresponding points minimizes the Monge-Kantorovich cost, Eq. (2), and it can be proven that these regions form a Laguerre diagram [26–29], a set of  $N$  convex polyhedral cells  $V_i^\psi$  defined by

$$V_i^\psi = \left\{ \mathbf{q} \mid \frac{1}{2} |\mathbf{x}_i - \mathbf{q}|^2 - \psi_i < \frac{1}{2} |\mathbf{x}_j - \mathbf{q}|^2 - \psi_j, \forall j \neq i \right\}, \quad (4)$$

where  $\psi$  is a vector of  $N$  scalars that corresponds to the gravitational potential at  $\tau_F$ . The Laguerre cells corresponding to each particle  $\mathbf{x}(\tau_F)$  collectively tessellate space as illustrated in Fig. 1.

In our case, the vector  $\psi$  that determines the Laguerre diagram can be obtained uniquely as the solution to the dual of the initial Monge-Kantorovich optimization problem,

$$K(\psi) = \sum_i \int_{V_i^\psi} \left[ \frac{1}{2} |\mathbf{x}_i - \mathbf{q}|^2 - \psi_i \right] d^3q + \frac{1}{N} \sum_i \psi_i, \quad (5)$$

subject to  $V_i^\psi \neq \emptyset, \forall i$ . Finally,  $\psi$ , the gravitational potential at  $\tau_F$ , is related to the gravitational potential

$\phi$  at  $\tau_I$  via the Legendre transform,

$$\begin{aligned} \phi(\tau_I, \mathbf{q}) &= \inf_{\mathbf{x}_F} \left[ \frac{1}{2} |\mathbf{q} - \mathbf{x}_i|^2 - \psi_i \right] = \\ &= \frac{1}{2} |\mathbf{q} - \mathbf{x}_{i(\mathbf{q})}|^2 - \psi_{i(\mathbf{q})}, \end{aligned} \quad (6)$$

where  $i(\mathbf{q})$  is the index of the Laguerre cell  $V_i$  that contains  $\mathbf{q}$ . In other words, maximizing  $K(\psi)$  is equivalent to solving for the gravitational potential  $\phi$  in the Monge-Ampère equation. The objective function  $K$  is concave [26–29], which ensures the existence and uniqueness of  $\psi$ , and  $C^2$ -smooth, which allows for an efficient and convergent optimization via a Newton algorithm [30]. It is the combination of these analytic properties of  $K$  that replaces the expensive combinatorial computation of previous methods with a Newton method that exploits the first- and second-order derivatives of  $K$  to efficiently minimize it.

Finally, each Laguerre cell  $V_i^\psi$  at  $\tau_I$  is mapped to its corresponding point  $\mathbf{x}_i$  at  $\tau_F$ . At an intermediate time  $\tau$  the trajectories of the mass elements can be deduced via a Lagrangian perturbation theory (LPT) description, in our case chosen to be the Zel'dovich approximation. This, in turn, can be converted as a mass density on a Eulerian grid, as depicted in Fig. 1 (see also [14]). In the following section we demonstrate the close agreement of reconstructed density fields with their respective input linear density fields for a set of simulations; particular attention is paid to the increased accuracy with which the acoustic scale can be recovered after reconstruction.

### III. BAO RECONSTRUCTION

Baryonic Acoustic Oscillations imprint a signature in the matter power spectrum by periodically modulating the large-scale power at a frequency corresponding to the sound horizon at decoupling in the real-space matter correlation function [1]. Non-linear gravitational evolution blurs and shifts this feature [4], complicating reliable detection and interpretation, wherefore reconstruction algorithms were devised that correct for such influences. In addition to physical effects, finite survey volumes, both in simulations and in practice, induce sample variance (so-called cosmic variance) into the measured quantities due to a reduced number of modes on these very scales. Since this variance is dominated by the un-modulated power spectrum, suites of dedicated  $N$ -body simulations are able to effectively cancel cosmic variance for analyses that only target the BAO signal [31–33], such as precision studies of reconstruction methods as done here. In this view, we apply our reconstruction algorithm [14] to the **FastPM** [15] simulations of Ref. [34].

This suite of **FastPM** simulations is comprised of pairs of simulations initiated with the same random phases at redshift  $z = 9$ , yet with power spectra that differ by the

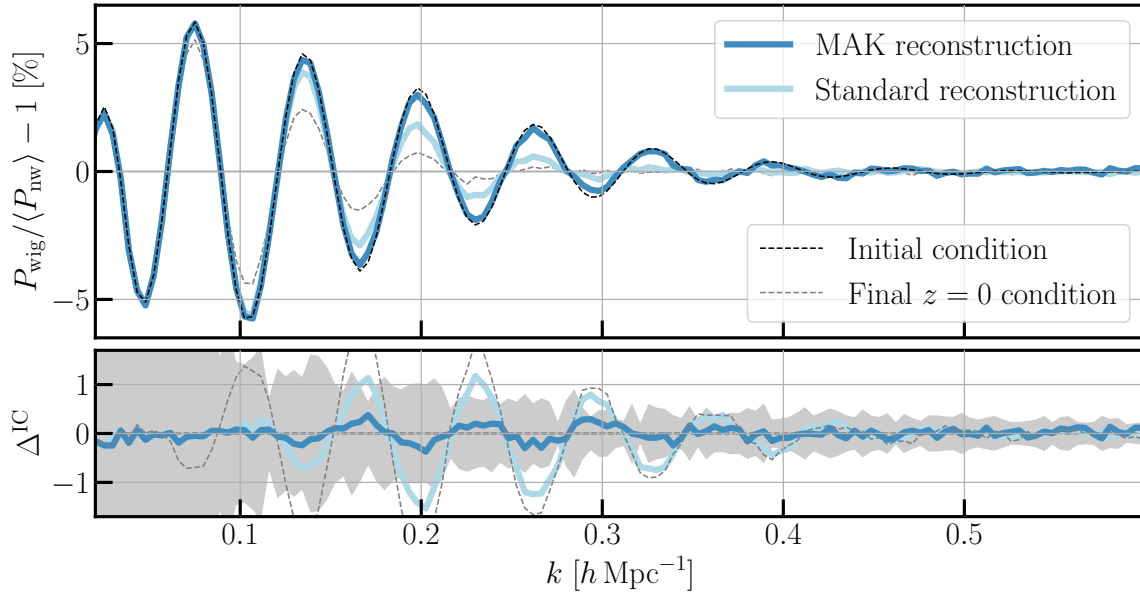


FIG. 2. Fractional BAO signal in simulations and reconstructions. *Top panel:* Ratio of power spectra from simulations with and without BAO signal, averaged over ten FastPM simulations and their reconstructions,  $\langle P_{\text{wig}}(k) - P_{\text{nw}}(k) \rangle / \langle P_{\text{wig}}(k) \rangle$ . *Bottom panel:* Deviations from the initial condition’s fractional BAO signal,  $\Delta^{\text{IC}}(k) = \langle P_{\text{wig}}(k) \rangle / \langle P_{\text{nw}}(k) \rangle - \langle P_{\text{wig}}^{\text{IC}}(k) \rangle / \langle P_{\text{nw}}^{\text{IC}}(k) \rangle$ . The shaded band indicates the standard deviation  $\sigma^{\text{IC}}(k)$  as estimated from the simulations and defined in the text.

presence of the BAO feature, in the following referred to as ‘wiggle’ and ‘no-wiggle’ power spectra, or  $P_{\text{wig}}(k)$  and  $P_{\text{nw}}(k)$ , respectively. Each of the simulations traces  $2048^3$  particles in a cube of  $1380 h^{-1} \text{Mpc}$  side length, simulated with 120 time steps between  $z = 9$  and  $z = 0$ , and saved at redshifts  $z = 0$  and  $z = 0.6$  as particle samples. In order to keep computing time low, we sub-sample only  $\sim 1\%$  of all particles in each of the ten simulation pairs we consider, which results in about  $85 \times 10^6$  particles per simulation. All simulations follow a  $\Lambda \text{CDM}$  cosmology with parameters from Ref. [35], which gives an expected BAO scale of  $r_{\text{BAO}}^{\text{th}} = 147.5 \text{Mpc}$ .

Beginning with these particles’ positions,  $\mathbf{x}$ , at  $z = 0$ , we compute the corresponding Laguerre diagram as described in the previous section, that in turn allows the computation of the density field at a given redshift. In order to compare with the simulations’ initial density fields at  $z = 9$  we evolve [14] the Laguerre cells to the same redshift via the choice of an appropriate linear growth factor [36]. Figure 2 demonstrates the effectiveness of our reconstruction, where the relative differences,  $d(k) = P_{\text{wig}}(k) / \langle P_{\text{nw}}(k) \rangle - 1$ , of initial ( $z = 9$ ) and final ( $z = 0$ ) power spectra are compared with those of our reconstructed density fields, averaged over all ten simulations. Our reconstruction’s excellent performance is further highlighted by contrasting it against the result obtained from so-called standard reconstruction [5][37], visible through the agreement of initial condition and reconstruction out to wave numbers  $k \gg 0.15 h^{-1} \text{Mpc}$ ,

where discrepancies between initial condition and standard reconstruction first appear.

In line with Ref. [32] we finally  $\chi^2$ -fit templates,  $m(k)$ , to the power spectrum ratios to obtain estimates of the BAO scale in each of the ten simulations. To this effect, we define  $m(k) = e^{k^2 \Sigma^2 / 2} [P_{\text{wig}}^{\text{IC}}(k/\alpha) / P_{\text{nw}}^{\text{IC}}(k/\alpha) - 1]$  as the relative difference of power spectra of the initial, linear density field, allowing for a shift  $\alpha = \hat{r}_{\text{BAO}} / r_{\text{BAO}}^{\text{th}}$  of the BAO scale, and a Gaussian damping  $\Sigma$  [38], and up-weight small scales via choice of the standard error  $\sigma^2(k) = 2 \text{Var}[d(k)] / N_{\text{modes}}(k)$ , where  $N_{\text{modes}}(k)$  is the number of Fourier modes that contribute to the computed power in each  $k$ -bin. We perform the fits over the full  $k$ -range shown in Figure 2, and the best-fit values of  $\alpha$  finally define the best-fit BAO scales  $\hat{r}_{\text{BAO}}$  in each fractional power spectrum  $d(k)$ . Table I presents biases and uncertainties in retrieving  $r_{\text{BAO}}^{\text{th}}$  in each of the simulations and reconstructions. While the comparison with the theory value  $r_{\text{BAO}}^{\text{th}}$  (left columns) confirms and restates more precisely the results of Ref. [14], the right columns optimally and for the first time showcase our algorithm’s accuracy and precision in reconstructing the BAO scale from noiseless cosmological simulations, by subtracting from each simulation the inherent BAO scale,  $r_{\text{BAO}}^{\text{IC}}$ , before determining mean and spread, thereby cancelling cosmic variance.

Due to the arising of shift terms in the non-linear power spectra [4, 32, 39], the BAO scale at  $z = 0$  appears biased by  $\sim 0.3\%$ , in accordance with previous find-

TABLE I. Bias and uncertainties of BAO scales recovered in the fractional power spectra of simulations and reconstructions with and without cancelling cosmic variance. The columns lists the mean values and standard deviations of  $r_{\text{BAO}}$  (*left columns*)  $r_{\text{BAO}} - r_{\text{BAO}}^{\text{IC}}$  (*right columns*) obtained from fitting  $\alpha$  to the power spectra as described in the main body.

	$\langle \hat{r}_{\text{BAO}} \rangle$ [Mpc]				$\sigma_{\hat{r}_{\text{BAO}}}$ [Mpc]			
	vs. theory		vs. IC		vs. theory		vs. IC	
Initial cond.	+0.02	[+0.01%]	$\pm 0.00$	[ $\pm 0.00\%$ ]	0.34	[0.23%]	0.00	[0.00%]
MAK rec.	-0.11	[-0.08%]	-0.13	[-0.09%]	0.44	[0.30%]	0.29	[0.19%]
Standard rec.	-0.03	[-0.02%]	-0.05	[-0.03%]	0.69	[0.47%]	0.85	[0.58%]
Final cond.	+0.48	[+0.33%]	+0.46	[+0.31%]	1.06	[0.72%]	1.19	[0.81%]

ings [32, 40, 41]. This is accompanied by a  $\sim 0.8\%$  uncertainty that reflects the blurring of the BAO peak that as well is caused by non-linear gravitational growth. Reconstruction reduces this bias [39] as we too see in both MAK and standard reconstruction, and further sharpens the BAO peak increasing the precision with which  $\hat{r}_{\text{BAO}}$  is determined; compared with the inherent uncertainty the simulations carry at the final condition – including cosmic variance – standard reconstruction improves the precision by a factor of 1.5 while MAK reconstruction gives a factor of 2.4 of enhancement. In an idealised scenario, without cosmic variance, the factor 1.4 improvement of standard reconstruction is surpassed by MAK reconstruction by as much as 4.3. In all cases we find a significant reduction of the bias as well. We expect even greater improvement from our method as soon as higher-order corrections are implemented into the trajectories of mass elements contained in the Laguerre cells.

As elaborated in Ref. [14], subsample variance (variance in the power spectrum due to the particular sample of particles) has significant impact on the overall error budget. Both shot noise and subsample variance are virtually removed by the use of the present simulation suite, and cosmic variance is further cancelled by direct simulation-to-simulation comparison as we display in the right columns, Table I. We therewith optimally test reconstructions’ accuracy.

#### IV. CONCLUSIONS

This *Letter* demonstrates the application of Optimal Transport theory to a specific problem in cosmology, the reconstruction of the BAO peak in the matter power spectrum from low- $z$  observations. BAO analyses play a crucial role in inferring cosmological parameters, and reconstruction methods have long aided the accuracy with which this signal is extracted. Outperforming many of the most promising algorithms, our method scales well ( $\propto N \log N$ ) with increased survey size, securing bright prospects in light of upcoming large-scale galaxy surveys.

In particular, we found that our reconstruction improves on detecting the BAO signal in the 2-point correlation function by a factor of 4.3 compared with attempting to extract the BAO scale without having performed any

reconstruction. Even in the case of having applied the so-called standard reconstruction technique, our method reduces the uncertainties by more than a factor of 3. This is highly promising especially given that in moving forward in time, we considered no more than the Zel’dovich approximation. We therefore highly anticipate further improvement of reported accuracy by amending the second step in Fig. 1 with corrections from higher-order perturbation theory à la Ref. [32, 42].

The next steps for optimal incorporation of our reconstruction method into analyses of survey data include its adaptation to account for the surveys’ selection functions, halo masses, redshift-space distortions, and characterization and computation of the reconstruction covariance matrices. Our algorithm’s flexibility easily accommodates such modifications without losing its efficiency.

In summary, our method makes direct use of the variational nature of gravitational evolution and thereby its reconstruction. It finds a quick path to the solution by leveraging first and second order information of the problem (*i.e.* it being both smooth ( $C^2$ ) and convex), while existing MAK methods need to exhaustively explore a huge ( $N^2 \log(N)$ ) combinatorial space. This is made possible by a fortuitous yet elegant convergence between the physical, mathematical and computational aspects of the problem: the specific cosmological setting that we considered (continuous mass transported to a point set) has nice mathematical properties (semi-discrete Monge-Ampère equation translated into a smooth and concave optimization problem), with an underlying geometric structure (Laguerre diagram) that can be *exactly* computed by our algorithm.

#### ACKNOWLEDGMENTS

The authors thank Zhejie Ding for sharing their simulations. SvH thanks Yu Feng for assistance with FastPM. BL and SvH acknowledge support from an Inria internal grant (Action exploratoire AeX EXPLORAGRAM). SvH is supported at Oxford by the Carlsberg Foundation, and wishes to thank Linacre College for the award of a Junior Research Fellowship. RM thanks the Rudolf Peierls Centre for hospitality.

- 
- [1] A. D. Sakharov, The Initial Stage of an Expanding Universe and the Appearance of a Nonuniform Distribution of Matter, *Soviet Journal of Experimental and Theoretical Physics* **22**, 241 (1966).
  - [2] R. A. Sunyaev and Y. B. Zeldovich, Small-Scale Fluctuations of Relic Radiation, *Astrophysics and Space Science* **7**, 3 (1970).
  - [3] P. J. E. Peebles and J. T. Yu, Primeval Adiabatic Perturbation in an Expanding Universe, *Astrophys. J.* **162**, 815 (1970).
  - [4] D. J. Eisenstein, H.-J. Seo, and M. J. White, On the Robustness of the Acoustic Scale in the Low-Redshift Clustering of Matter, *Astrophys. J.* **664**, 660 (2007), arXiv:astro-ph/0604361.
  - [5] D. J. Eisenstein, H.-J. Seo, E. Sirko, and D. Spergel, Improving Cosmological Distance Measurements by Reconstruction of the Baryon Acoustic Peak, *Astrophys. J.* **664**, 675 (2007), arXiv:astro-ph/0604362 [astro-ph].
  - [6] S. Cole, W. J. Percival, J. A. Peacock, P. Norberg, C. M. Baugh, C. S. Frenk, I. Baldry, J. Bland-Hawthorn, T. Bridges, R. Cannon, *et al.*, The 2dF Galaxy Redshift Survey: power-spectrum analysis of the final data set and cosmological implications, *MNRAS* **362**, 505 (2005), arXiv:astro-ph/0501174 [astro-ph].
  - [7] D. J. Eisenstein, I. Zehavi, D. W. Hogg, R. Scoccimarro, M. R. Blanton, R. C. Nichol, R. Scranton, H.-J. Seo, M. Tegmark, Z. Zheng, *et al.*, Detection of the Baryon Acoustic Peak in the Large-Scale Correlation Function of SDSS Luminous Red Galaxies, *Astrophys. J.* **633**, 560 (2005), arXiv:astro-ph/0501171 [astro-ph].
  - [8] G.-B. Zhao, Y. Wang, S. Saito, H. Gil-Marín, W. J. Percival, D. Wang, C.-H. Chuang, R. Ruggeri, E.-M. Mueller, F. Zhu, *et al.*, The clustering of the SDSS-IV extended Baryon Oscillation Spectroscopic Survey DR14 quasar sample: a tomographic measurement of cosmic structure growth and expansion rate based on optimal redshift weights, *MNRAS* **482**, 3497 (2019), arXiv:1801.03043 [astro-ph.CO].
  - [9] D. Baumann, D. Green, and M. Zaldarriaga, Phases of New Physics in the BAO Spectrum, *JCAP* **2017** (11), 007, arXiv:1703.00894 [astro-ph.CO].
  - [10] To date, these include, but are not limited to, *e.g.*, DESI [43], LSST [44], Euclid [45].
  - [11] C. Villani, *Optimal transport : old and new*, Grundlehren der mathematischen Wissenschaften (Springer, Berlin, 2009).
  - [12] C. Villani, *Topics in optimal transportation*, Graduate studies in mathematics (American Mathematical Society, Providence (R.I.), 2003).
  - [13] U. Frisch, S. Matarrese, R. Mohayaee, and A. Sobolevskii, A reconstruction of the initial conditions of the universe by optimal mass transportation, *Nature* **417** (2002).
  - [14] B. Levy, R. Mohayaee, and S. von Hausegger, A fast semidiscrete optimal transport algorithm for a unique reconstruction of the early Universe, *MNRAS* **506**, 1165 (2021), arXiv:2012.09074 [astro-ph.CO].
  - [15] Y. Feng, M.-Y. Chu, U. Seljak, and P. McDonald, FastPM: a new scheme for fast simulations of dark matter and haloes, *MNRAS* **463**, 2273 (2016), arXiv:1603.00476 [astro-ph.CO].
  - [16] Y. Brenier, U. Frisch, M. Henon, G. Loeper, S. Matarrese, R. Mohayaee, and A. Sobolevskii, Reconstruction of the early universe as a convex optimization problem, *MNRAS* **346**, 501 (2003), arXiv:astro-ph/0304214.
  - [17] L. Landau and E. Lifshitz, *Course of Theoretical Physics, Volume 1: mechanics* (Butterworth-Heinemann, 1975).
  - [18] Y.-B. Zel'dovich, Gravitational instability: an approximate theory for large density perturbations, *Astronomy and astrophysics* **5**, 84 (1970).
  - [19] J. Benamou and Y. Brenier, A computational fluid mechanics solution to the monge-kantorovich mass transfer problem, *Numerische Mathematik* **84**, 375 (2000).
  - [20] G. Monge, Mémoire sur la théorie des déblais et des remblais, *Histoire de l'Académie Royale des Sciences* (1781), 666 (1784).
  - [21] Y. Brenier, Polar factorization and monotone rearrangement of vector-valued functions, *Communications on Pure and Applied Mathematics* **44**, 375 (1991).
  - [22] Y. Shi, M. Cautun, and B. Li, New method for initial density reconstruction, *Phys. Rev. D* **97**, 023505 (2018), arXiv:1709.06350 [astro-ph.CO].
  - [23] J. Birkin, B. Li, M. Cautun, and Y. Shi, Reconstructing the baryon acoustic oscillations using biased tracers, *MNRAS* **483**, 5267 (2019), arXiv:1809.08135 [astro-ph.CO].
  - [24] Y. Liu, Y. Yu, and B. Li, Biased Tracer Reconstruction with Halo Mass Information, *Astrophys. J. Suppl.* **254**, 4 (2021), arXiv:2012.11251 [astro-ph.CO].
  - [25] D. P. Bertsekas, Auction algorithms for network flow problems: A tutorial introduction, *Computational Optimization and Applications* **1**, 7 (1992).
  - [26] F. Aurenhammer, F. Hoffmann, and B. Aronov, Minkowski-type theorems and least-squares partitioning, in *Symposium on Computational Geometry* (1992) pp. 350–357.
  - [27] Q. Mérigot, A multiscale approach to optimal transport, *Comput. Graph. Forum* **30**, 1583 (2011).
  - [28] B. Lévy, A numerical algorithm for  $L_2$  semi-discrete optimal transport in 3d, *ESAIM M2AN (Mathematical Modeling and Analysis)* (2015).
  - [29] Q. Mérigot and B. Thibert, Optimal transport: discretization and algorithms (2020), arXiv:math/2003.00855 [math.OC].
  - [30] J. Kitagawa, Q. Mérigot, and B. Thibert, A newton algorithm for semi-discrete optimal transport, *CoRR* (2016), arXiv:1603.05579.
  - [31] F. Prada, C. G. Scóccola, C.-H. Chuang, G. Yepes, A. A. Klypin, F.-S. Kitaura, S. Gottlöber, and C. Zhao, Hunting down systematics in baryon acoustic oscillations after cosmic high noon, *MNRAS* **458**, 613 (2016), arXiv:1410.4684 [astro-ph.CO].
  - [32] M. Schmittfull, T. Baldauf, and M. Zaldarriaga, Iterative initial condition reconstruction, *Phys. Rev. D* **96**, 023505 (2017), arXiv:1704.06634 [astro-ph.CO].
  - [33] X. Wang, H.-R. Yu, H.-M. Zhu, Y. Yu, Q. Pan, and U.-L. Pen, Isobaric Reconstruction of the Baryonic Acoustic Oscillation, *Astrophys. J. Lett.* **841**, L29 (2017), arXiv:1703.09742 [astro-ph.CO].
  - [34] Z. Ding, H.-J. Seo, Z. Vlah, Y. Feng, M. Schmittfull, and F. Beutler, Theoretical Systematics of Future Baryon Acoustic Oscillation Surveys, *MNRAS* **479**, 1021 (2018), arXiv:1708.01297 [astro-ph.CO].

- [35] P. A. R. Ade *et al.* (Planck), Planck 2015 results. XIII. Cosmological parameters, *Astron. Astrophys.* **594**, A13 (2016), arXiv:1502.01589 [astro-ph.CO].
- [36] The present analysis is not very sensitive to the choice of growth factor [46] as it is only concerned with the ratio of ‘wiggles’ and ‘no-wiggles’ simulations.
- [37] We computed the standard reconstructed density field using the routine `FFTRecon` of the `python` suite `nbbodykit` [47].
- [38] We define  $P_{\text{wig}}^{\text{IC}}(k/\alpha)/P_{\text{nw}}^{\text{IC}}(k/\alpha)$  as the average over all ten simulations, shown in Fig. 2, and interpolated to accommodate values of  $\alpha \neq 1$ .
- [39] B. D. Sherwin and M. Zaldarriaga, Shift of the baryon acoustic oscillation scale: A simple physical picture, *Phys. Rev. D* **85**, 103523 (2012), arXiv:1202.3998 [astro-ph.CO].
- [40] H.-J. Seo, J. Eckel, D. J. Eisenstein, K. Mehta, M. Metchnik, N. Padmanabhan, P. Pinto, R. Takahashi, M. White, and X. Xu, High-precision Predictions for the Acoustic Scale in the Nonlinear Regime, *Astrophys. J.* **720**, 1650 (2010), arXiv:0910.5005 [astro-ph.CO].
- [41] K. T. Mehta, H.-J. Seo, J. Eckel, D. J. Eisenstein, M. Metchnik, P. Pinto, and X. Xu, Galaxy Bias and Its Effects on the Baryon Acoustic Oscillation Measurements, *Astrophys. J.* **734**, 94 (2011), arXiv:1104.1178 [astro-ph.CO].
- [42] F. Bernardeau, S. Colombi, E. Gaztanaga, and R. Scoccimarro, Large scale structure of the universe and cosmological perturbation theory, *Phys. Rept.* **367**, 1 (2002), arXiv:astro-ph/0112551.
- [43] DESI Collaboration, A. Aghamousa, J. Aguilar, S. Ahlen, S. Alam, L. E. Allen, C. Allende Prieto, J. Annis, S. Bailey, *et al.*, The DESI Experiment Part I: Science, Targeting, and Survey Design, arXiv e-prints , arXiv:1611.00036 (2016), arXiv:1611.00036 [astro-ph.IM].
- [44] LSST Dark Energy Science Collaboration, Large Synoptic Survey Telescope: Dark Energy Science Collaboration, arXiv e-prints , arXiv:1211.0310 (2012), arXiv:1211.0310 [astro-ph.CO].
- [45] Euclid Collaboration, R. Laureijs, J. Amiaux, S. Arduini, J. L. Auguères, J. Brinchmann, R. Cole, M. Cropper, C. Dabin, L. Duvet, *et al.*, Euclid Definition Study Report, arXiv e-prints , arXiv:1110.3193 (2011), arXiv:1110.3193 [astro-ph.CO].
- [46] Z. Lukic, K. Heitmann, S. Habib, S. Bashinsky, and P. M. Ricker, The Halo Mass Function: High Redshift Evolution and Universality, *Astrophys. J.* **671**, 1160 (2007), arXiv:astro-ph/0702360.
- [47] N. Hand, Y. Feng, F. Beutler, Y. Li, C. Modi, U. Seljak, and Z. Slepian, nbbodykit: an open-source, massively parallel toolkit for large-scale structure, *Astron. J.* **156**, 160 (2018), arXiv:1712.05834 [astro-ph.IM].